San Jose State University
SJSU ScholarWorks

Master's Theses   Master's Theses and Graduate Research

2002

Hyperspectral remote sensing of subtidal macrophytes in optically shallow water

Sara K. Wittlinger
San Jose State University

Follow this and additional works at: https://scholarworks.sjsu.edu/etd_theses

INFORMATION TO USERS

This manuscript has been reproduced from the microfilm master. UMI films the text directly from the original or copy submitted. Thus, some thesis and dissertation copies are in typewriter face, while others may be from any type of computer printer.

The quality of this reproduction is dependent upon the quality of the copy submitted. Broken or indistinct print, colored or poor quality illustrations and photographs, print bleedthrough, substandard margins, and improper alignment can adversely affect reproduction.

In the unlikely event that the author did not send UMI a complete manuscript and there are missing pages, these will be noted. Also, if unauthorized copyright material had to be removed, a note will indicate the deletion.

Oversize materials (e.g., maps, drawings, charts) are reproduced by sectioning the original, beginning at the upper left-hand corner and continuing from left to right in equal sections with small overlaps.

UMI®

HYPERSPECTRAL REMOTE SENSING OF SUBTIDAL MACROPHYTES IN OPTICALLY SHALLOW WATER

A Thesis

Presented to

The Faculty of Moss Landing Marine Laboratories

San Jose State University

In Partial Fulfillment

of the Requirements for the Degree

Master of Science

by

Sara K. Wittlinger

August 2002

UMI Number: 1410453

UMI®

APPROVED FOR THE DEPARTMENT OF BIOLOGY

Dr. Michael S. Foster, Moss Landing Marine Laboratories

Dr. Richard C. Zimmerman, Moss Landing Marine Laboratories

Dr. William W. Broenkow, Moss Landing Marine Laboratories

APPROVED FOR THE UNIVERSITY

ABSTRACT

HYPERSPECTRAL REMOTE SENSING OF SUBTIDAL MACROPHYTES IN OPTICALLY SHALLOW WATER

by Sara K. Wittlinger

Remote sensing offers an alternative to diver surveys for the large-scale inventory of benthic macrophytes in the shallow subtidal environment. The goal of this study was to determine the limits of spectral discrimination of benthic macrophytes as a function of depth and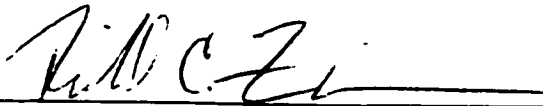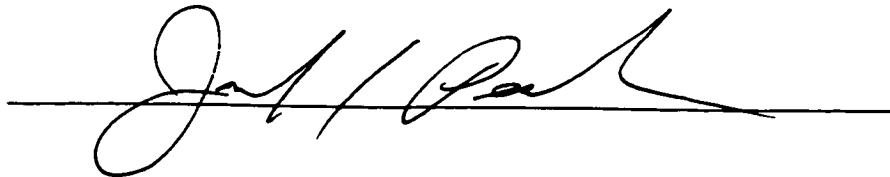 water clarity. Bottom reflectance and water column optical properties were measured to predict the capabilities of remote sensing reflectance to distinguish classes of benthic vegetation. These predictions were compared to in situ surface measures of remote sensing reflectance. Bottom reflectance was separated into five optical classes, based on spectral shape and amplitude: fleshy red algae, coralline red algae, brown algae, seagrass, and sand. Characteristic peaks of bottom reflectance were clearly maintained in the remote sensing reflectance spectra at wavelengths below 600 nm and can provide the basis for identification of bottom vegetation from remote sensing reflectance in depths of 2 to 4 meters, depending on water clarity.

ACKNOWLEDGMENTS

TABLE OF CONTENTS

LIST OF TABLES

LIST OF FIGURES

LIST OF APPENDICES

The shallow subtidal waters of the coastal zone contain a diverse array of benthic vegetation. In some cases, the vegetation provides the foundation of the local ecosystem such as seagrasses in sheltered tropical and temperate waters (Hemminga and Duarte 2000) and seaweed assemblages in temperate rocky environments (Foster and Schiel 1985). In other cases, the vegetation may be invasive or destructive to the natural ecosystem such as the invasion of *Caulerpa taxifolia* in the Mediterranean (Meinesz et al. 1993) and its more recent discovery in a lagoon and harbor in southern California (Jousson et al. 2000; Kaiser 2000) or macroalgal blooms on coral reefs (Hughes 1994). Defining the abundance and distribution of natural and anthropogenically altered assemblages of subtidal macrophytes is important for ecological studies and resource management. The abundance and distribution of subtidal organisms have traditionally been measured using diver surveys, which are time-consuming and thus limited in areal and temporal coverage. Remote sensing offers a potential alternative to diver surveys for the large-scale inventory of benthic photosynthetic organisms such as macroalgae, seagrasses, and corals (Jupp et al. 1985).

The challenge in detecting benthic vegetation by remote sensing is that bottom reflectance is distorted by the water column, so that the spectral characteristics of bottom reflectance become more difficult to detect as depth and turbidity increase. The remote sensing reflectance of aquatic environments is the ratio of the water leaving radiance (L_w) to the downward irradiance incident on the water's surface. The water leaving radiance is about 54% that of the upward radiance (L_u) just below the surface, due to reflection and refraction as light passes through the water-air boundary (Kirk 1994). In optically

1

shallow water, where bottom reflectance has a measurable impact on water leaving radiance, the upward radiance just below the surface is dependent on the reflectance of the benthic boundary, the optical properties of the water column, and the water depth.

Maritorena et al. (1994) described the reflectance [$R(0,H)$] just below the surface of a uniform ocean bounded by a reflecting bottom at depth H as:

$$R(0,H) = R_\infty + (A-R_\infty)\exp(-2KH) \qquad (1)$$

where R_∞ is the reflectance of an infinitely deep ocean, A is the bottom albedo or reflectance, K is an aggregated coefficient for both downwelling and upwelling attenuation, and H is the bottom depth in meters (Table 1). All terms except H are implicitly spectral and the descriptor "λ" has been omitted for brevity. The reflectance of optically shallow water approaches R_∞ as bottom depth increases, but as H decreases, the contrast between the bottom albedo and deep ocean reflectance ($A-R_\infty$) becomes more important in the remotely sensed signal. It is this contrast that allows vegetated bottoms to be differentiated from optically deep water. Similarly, it is the contrast in bottom albedo (A_1-A_2) that dictates the limits of distinguishing between two different bottom types.

Satellite mounted multispectral sensors have been used to map large coral reefs in clear, shallow water (Jupp et al. 1985; Knight et al. 1997). However, the spatial resolution of satellite data, which is on the order of tens to thousands of meters, is too coarse for many coastal applications where the scale of important bottom features are on the order of one meter (Mumby et al. 1997). Increased spatial resolution reduces the number of heterogeneous, or mixed, pixels that compound the difficulty of identifying

benthic components and were not considered in this study. Thus, fine spatial resolution becomes increasingly important in benthic environments with small-scale mixing of vegetative types.

Spatial resolution can be greatly increased by mounting sensors on aircraft and measuring the remote sensing reflectance from a low altitude. Species of emergent and floating vegetation in a lake with a maximum depth of four meters were differentiated using three bands from an airborne thematic mapper (Malthus and George 1997). Because two of the bands used in this analysis were in the infrared wavelengths, which are strongly absorbed by water, the signals of the submerged species were not detectable and could not be mapped. However, during the field portion of this same study by Malthus and George (1997), shallow submerged species were identified using a high resolution (~11 nm resolution) spectroradiometer held above the surface of the water.

High spectral resolution is also necessary to distinguish the small spectral differences between benthic components. Narrower bands make it possible to distinguish reflectance peaks that would otherwise be averaged out in wider spectral bands. Bajjouk et al. (1996) used an aircraft mounted multispectral sensor with narrow bands (7 to 20 nm) to successfully distinguish between exposed intertidal brown, red and green algae during a low tide. In a comparison of remote sensing methods, the sensor with the largest number of spectral bands provided the most accurate data in mapping an area of coral reef, seagrass beds, algae, and sand (Mumby et al. 1997).

Hyperspectral sensors may provide the spectral sensitivity required for distinguishing between classes of submerged benthic macrophytes. Hyperspectral

sensors have a large number of narrow contiguous spectral bands, in contrast to multispectral sensors that have fewer, larger bands and incomplete coverage of the spectrum due to wavelength gaps. Another advantage of hyperspectral data is that they are continuous across the spectrum, allowing the use of derivative analysis which may be helpful in determining spectral peaks, resolving overlapping spectra, and providing additional information such as vegetation health and accessory pigment composition (Demetriades-Shah et al. 1990; Peñuelas et al. 1993; Richardson et al. 1994).

The objective of this study was to quantify the ability of hyperspectral remote sensing to distinguish optical classes of subtidal macrophytes (seagrasses and seaweeds) from optically deep water, and from one another, as a function of water clarity and depth. Because remote sensing reflectance retains more of the characteristic spectra of the bottom reflectance in clearer than in turbid water, many remote sensing studies have focused on the ability to detect benthic vegetation or coral reefs in clear, tropical waters (Armstrong 1993; Knight et al. 1997; Mumby et al. 1997). In this study, I broaden the analysis of hyperspectral remote sensing to include the more turbid conditions characteristic of temperate coastal waters that contain significant amounts of dissolved and suspended particulate matter.

To accomplish these objectives, the spectral signatures of optical classes of subtidal macrophytes including fleshy red algae (non-calcareous red seaweed), coralline red algae (with calcified thalli), brown algae, and green seagrass were identified to provide bottom reflectance for the radiative transfer model. Radiative transfer theory was used to evaluate upward propagation of bottom reflectance as a function of depth and the

4

measured optical properties of the water. Theoretical calculations were compared to field measures of remote sensing reflectance to evaluate the utility of hyperspectral data to characterize optically shallow waters. Once the measurements were validated, they were used to evaluate the detection limits of optically shallow bottoms. Finally, characteristic spectral features were extracted from field data to identify the benthic composition of an area based on its remote sensing reflectance.

METHODS

Study site – Field studies were conducted in two areas along the Monterey Peninsula in central California (Fig. 1). The first area was along the north shore of the Peninsula in the waters of Monterey Bay adjacent to the cities of Monterey and Pacific Grove, CA (36°36' N, 121°53' W to 36°37' N, 121°54' W). The second site was along the south shore of the Peninsula in Stillwater Cove (36°33' N, 121°56' W). In both areas, a variety of brown, fleshy red and coralline algal species covered all of the subtidal rocky substrate.

The study areas are dominated by giant kelp, *Macrocystis pyrifera*, (for a description see Foster and Schiel 1985) which forms a surface canopy throughout much of the year. This study does not address reflectance from the surface canopy, which emits a strong infrared signal that is easily identified in remote sensing data sets and has traditionally been mapped using infrared aerial photography (Jensen et al. 1980; Hernández-Carmona et al. 1989) and more recently using multispectral remote sensing

(Deysher 1993). The focus of my study is the understory macroalgal reflectance as modified by the overlying water column in the absence of a surface kelp canopy.

The brown macroalgae examined in this study were primarily kelps from the Order Laminariales and had large laminar blades. The red macroalgae consisted of both fleshy red and coralline red algae. Morphology of the fleshy red algae ranged from small, highly branched to large paddle shaped thalli. The coralline red algae included both geniculate (articulated) and nongeniculate (crustose) forms. Subtidal green algae were very rare in the study area. Consequently, the seagrass *Zostera marina* (eelgrass), which is found in unconsolidated sediments of protected areas, was used to represent the green optical class in this analysis.

The waters surrounding the Monterey Peninsula are seasonally mesotrophic, with high chlorophyll concentrations during the upwelling period of spring and summer (Pennington and Chavez 2000). There is a strong detrital component from both resuspended sediments and terrestrial runoff in the winter.

Spectral library - Using SCUBA, multiple samples of eight species of fleshy red algae, three species of coralline red algae, and eight species of brown algae (Table 2) were collected from the study sites and stored in seawater for transport back to the laboratory. All species were common and abundant at the study sites with the exception of *Mesophyllum conchatum* which was found on only one occasion but was included to increase the sample size of coralline red algal species. Macroalgae were identified based on Abbott and Hollenberg (1976), with nomenclature changes based on more recent

literature. Samples of eelgrass were collected at Del Monte Beach near the northeast corner of the Monterey Peninsula using the same methods.

Tissue samples were blotted dry and reflectances were measured across the visible spectrum using a Shimadzu UV-2101PC spectrophotometer fitted with an integrating sphere that allows accurate spectral measurements of highly scattering media. Measurements were recorded at 1-nm intervals from 350 to 750 nm. Because of the spectral variation within species (Price 1994), the reflectance of multiple samples of each species was measured and averaged for the spectral library. The reflectance spectra of forty-five eelgrass leaves of all ages were averaged to represent the green optical class.

The reflectance of sand was also measured, as sand is often found in contrast to vegetated bottoms in the subtidal environment. The spectral signature of sand reflectance was based on an average of ten measurements made in Stillwater Cove using an underwater spectroradiometer that measures spectral downwelling irradiance (E_d) and upwelling irradiance (E_u) in situ (Zimmerman in review). The cosine collectors were positioned fifteen centimeters above the surface of the sand.

Water column inherent optical properties - Thirty-five seawater samples were collected over an eighteen month period in order to define the range of water column inherent optical properties (IOPs) in the study area. Seawater samples were collected in 1-L polycarbonate bottles from just below the surface and kept cold and dark during transport back to the laboratory. Water was filtered onto a 25-mm glass-fiber filter (Whatman GF/F) using a vacuum pressure of 5-mm Hg to avoid the breakage of cells. The optical density of the filter-collected phytoplankton and detritus was measured using

7

a Shimadzu UV-2101PC spectrophotometer fitted with an integrating sphere and baselined against a clean GF/F filter saturated with ultrapure (18 MΩ cm^{-1}) deionized water. Care was taken to keep the moisture content of the filters constant by maintaining a fixed time interval between the end of filtration and the shut down of the vacuum (3 s). The particle absorption coefficient (a_p) was corrected for multiple scattering according to Cleveland and Weidemann (1993).

The optical density of colored dissolved organic matter (CDOM) was measured in a quartz cuvette (10-cm pathlength) after removing particles by filtration through a 0.22-μm membrane filter (Nucleopore Corporation) at a vacuum pressure of 5-mm Hg. The CDOM absorption coefficient (a_y) was added to the particle absorption coefficient (a_p) to determine the total absorption coefficient (without water) at 1-nm intervals from 350 to 750 nm.

The beam attenuation coefficient (c) was determined by measuring the optical density of unfiltered seawater in the 10-cm quartz cuvette. Although c is best measured in situ, laboratory measurements made with a spectrophotometer are reliable if long-pathlength cells are used (Bochkov et al. 1980; Kirk 1994). As was done for measurements of a_y, the spectrophotometer was blanked with ultrapure (18 MΩ cm^{-1}) deionized water and measurements were recorded at 1-nm intervals from 350 to 750 nm. The scattering coefficient (b) was calculated as the difference between the beam attenuation coefficient ($c_{t-w} = c_y + c_p$) and the absorption coefficient ($a_{t-w} = a_y + a_p$).

Pigments were extracted by grinding the filter pad samples in ice cold 90 % acetone. The samples were centrifuged to pellet the debris and the absorbance of the

8

supernatant was measured in a 1-cm pathlength cuvette using the spectrophotometer blanked against 90% acetone. Phaeopigment was measured after the acidification of each sample with 3N HCl. Using the absorbance values at 665 nm and 750 nm, before and after acidification, the chlorophyll a and phaeopigment concentrations were calculated by applying the equations from Strickland and Parsons (1972). All stated pigment concentrations represent the combined concentrations of chlorophyll a + phaeopigment.

Modeled remote sensing reflectance - The radiative transfer model Hydrolight© was used to study the effects of bottom reflectance, water column optical properties, and depth on remote sensing reflectance (Mobley 1989). The model was used to predict the remote sensing reflectance of bottoms of algae, seagrass, and sand beginning at a depth of two meters and at increasing two meter depth increments until there was no apparent difference between the remote sensing reflectance of vegetated or sand bottoms and that of optically deep water. Bottom reflectance was provided from the spectral library and the water column IOPs chosen for use in the model were representative of all samples collected and processed as described above. The remote sensing reflectance of optically deep water was calculated for each set of water column IOPs as well.

Field measurements of remote sensing reflectance - A hyperspectral tethered spectral radiometer buoy (HTSRB, Satlantic, Inc.) was used to measure the remote sensing reflectance at the sea surface and test the predictions of the radiative transfer model. The HTSRB measures downwelling irradiance (E_d) in air and upwelling radiance (L_u) 0.6 m below the surface, at a rate of 1 Hz, from 395 to 795 nm with a 2.5 nm bandwidth. Field measurements were recorded for three minutes each over a variety of

homogeneous bottom types and in waters with varying depths and optical properties. The bottom type over which the HTSRB was deployed, determined visually by a diver, and the inherent optical properties (a and c) of water sampled at the site were used as parameters for validation of the model predictions. The HTSRB does not measure true remote sensing reflectance because it measures upwelling radiance at 0.6 meters below the surface, not water leaving radiance. The radiative transfer model, however, can predict upwelling radiance at any depth desired, allowing a comparison between the model predictions and actual measurements.

The Satlantic SatCon© software program was used to transform raw data into radiometric units. E_d and L_u were interpolated to common wavelengths and separated into five nanometer bins using an independently developed software program developed by D. Kohler (Cornell University). Instrument noise, measured by shuttered readings, was subtracted from the spectral signals during processing.

Analysis of environmental variability and detection limits - Environmental variability, resulting in variation in the amplitude of the remote sensing reflectance signal over time, was caused by wave focusing, buoy sway, and the lateral motion of the buoy producing subsequent changes in depth during the measurement period. Twenty-one HTSRB files, containing approximately 150 spectra each recorded over a variety of bottom types and in different water and weather conditions, were analyzed for equal variances. All variances were homoscedastic and therefore the mean signal of each file gave a reliable measurement of remote sensing reflectance. The percent error for each HTSRB file was determined by dividing the 95% confidence interval by the mean and the

10

resulting error spectra were averaged to calculate the average percent error that was caused by environmental variability.

This calculated field error was then applied to the modeled spectra to simulate variability and help to determine the limits of detection between the remote sensing reflectance spectra of two different bottom types. In order to discriminate between two spectra, the difference between the two signals must be at least double the possible error of the spectra (Willard et al. 1974). The error at 550 nm was used to calculate the detection limit between two different bottom types, or between benthic reflectance and optically deep water, as a function of optical depth. This wavelength was chosen because (i) it penetrates deeply into the water column; (ii) it is included in the green band of multispectral sensors such as SeaWIFS and MODIS (545-565 nm); and, (iii) there are large differences in the bottom reflectance of the optical classes (with the exception of the brown and fleshy red algae) at this wavelength.

Benthic identification – The HTSRB was towed at 2 knots along a 90 m transect in Stillwater Cove to collect remote sensing reflectance over a variety of subtidal habitats for analysis of bottom composition. Frame position was simultaneously recorded using a Magellan NAV 6000 Global Positioning System (GPS) receiver interfaced to the HTSRB control software. Characteristic spectral peaks, established as the wavelength of peak emission between 530 and 600 nm as predicted by the modeled spectra, were extracted from the field spectra and used to identify the bottom type of each spectral frame recorded by the HTSRB. The resulting transect of classified benthic vegetation was

overlaid on a false color image of remotely sensed data from a remote sensing aircraft overflight to show position within Stillwater Cove.

RESULTS

Spectral library – Bottom reflectance was separated into five optical classes, consisting of fleshy red algae, coralline red algae, brown algae, seagrass, and sand, based on differences in reflectance spectral shape and amplitude (Fig. 2, Appendix 1). The red, brown, green, and sand spectra separated out easily from one another based on shape, whereas the fleshy red and coralline red algae had similar spectral shapes due to common pigments. However, the fleshy red algae could be separated from the coralline red algae based on large differences in the amplitudes of their reflectance spectra. The coralline red algae had a higher overall reflectance (5 to 9 %) than the fleshy red algae (< 5%) and the ratio of red to green wavelengths (600/540 nm) was higher in the coralline red algae spectrum (2.0) than in the fleshy red algae spectrum (1.3). These two factors resulted in the coralline red algae appearing much brighter than the fleshy red algae in the red wavelengths.

Spectral properties of seaweeds and seagrasses are determined primarily by their photosynthetic pigments. Although all macrophytes contain chlorophyll *a*, it is the accessory pigments, which blend with or mask chlorophyll *a*, that give them their characteristic color and spectral properties. The fleshy red and coralline red algae contain the biliprotein pigments, phycoerythrin and phycocyanin. Phycoerythrin, which absorbs light between 540 and 565 nm, was responsible for the low reflectance of the red algae in

the green wavelengths. Both the fleshy red and coralline red algae spectra contained reflectance peaks at 600 and 645 nm that gave them their characteristic red color. The dip in reflectance around 620 nm was due to the broad absorption band of phycocyanin around this wavelength (Govindjee and Braun 1974).

The brown algae contain the accessory pigments chlorophyll c and the carotenoid fucoxanthin, which do not absorb well beyond 550 nm. As a result, there was an increased reflectance from 550 to 580 nm in the brown algal spectral signature that was absent in the reflectance spectra of the red algae. The amplitudes of the brown and fleshy red algal reflectance spectra were comparable at wavelengths in the blue and the green, at about four percent. However, the reflectance of the fleshy red algae was brighter than that of the brown algae from 585 to 665 nm due to the characteristic reflectance peaks of the red algae spectrum at 600 and 645 nm.

The eelgrass reflectance spectrum possessed a broad peak from about 530 to 565 nm, typical of green plants, due to low absorption by both chlorophylls a and b in this region. Eelgrass reflectance was brighter across the entire spectrum than that of the fleshy red and the brown algae. This enhanced reflectance may be due to the presence of lacunae, interstitial channels that allow gas transport through the leaves. The difference in the refractive index between the mesophyll cells and these gas-filled spaces should increase scattering within the leaf and result in higher overall reflectance of the eelgrass leaves.

The sand reflectance spectrum increased from blue to red with a slight dip at 675 nm due to absorption by microalgae present on the sand. Despite the relatively low

reflectance of this siliciclastic sand compared to its carbonate counterparts (Zimmerman in review), sand reflectance was brighter than that of all of the macrophytes, increasing from five percent in the blue region of the spectrum to ten percent in the red region. The brightness of sand provided a good contrast to the reflectance of the macrophyte classes examined in this study.

Water column inherent optical properties – Measured total pigment concentrations ranged from 0.5 mg m^{-3} to 22 mg m^{-3} in thirty-five samples collected around the Monterey Peninsula between July 1999 and December 2000. Total pigment concentration was highest during the late summer and early fall with the two highest concentrations occurring within three days of each other in the month of October 1999 (Fig. 3). Five water samples with total pigment concentrations of 1.0, 2.4, 4.9, 6.0, and 10.6 mg m^{-3} were selected to represent the usual range of water column optical properties for the radiative transfer calculations. Only two of the collected water samples had total pigment concentration higher than 10.6 mg m^{-3} and, due to the extreme turbidity of these samples, they were not used in the model. Although the water samples will be referred to in this paper by their pigment concentration, it is the spectral absorption, scattering, and beam attenuation coefficients (a, b, and c) that were used in the radiative transfer calculations.

The spectral absorption coefficient generally increased with pigment concentration but did not differ markedly for pigment concentrations of 1.0 to 6.0 mg m^{-3} (Fig. 4A). The absorption coefficient for the 10.6 mg m^{-3} sample, however, was two to three times greater than those of the other samples. Absorption coefficients in the blue

14

wavelengths were dominated by CDOM absorption, which was 40 to 80% of a_t at 450

nm and 40 to 60 % at 550 nm. Although the contribution of the particle (chlorophyll and

detritus) absorption to a_t was small at lower pigment concentrations of 1.0 and 2.4 mg m^{-3}

(< 25% at 450 nm and <15% at 550 nm), a significant portion of the total absorption

coefficient (about 50% at 450 nm and 25 to 35 % at 550 nm in this study) was due to

particle absorption at pigment concentrations of 4.9, 6.0 and 10.6 mg m^{-3}.

The scattering coefficient (b) did not show the same relationship to pigment

concentration as the absorption coefficient at wavelengths below 500 nm, indicating a

strong detrital component in the water column (Fig. 4B). Scattering generally increased

with increasing pigment concentration at wavelengths above 500 nm, except that b was

lower for the 2.4 mg m^{-3} sample than the 1.0 mg m^{-3}, indicating a higher detrital

component in the latter sample. The scattering coefficient for the 10.6 mg m^{-3} sample

was about twice as high as for the other samples across all wavelengths. The scattering

coefficients of the two samples with the lowest pigment concentrations (1.0 and 2.4 mg

m^{-3}) declined with increasing wavelength. However, the scattering coefficients of the

three samples with higher pigment concentration (4.9, 6.0, and 10.6 mg m^{-3}) possessed

dips at 440 and 670 nm that mirrored the distinctive chlorophyll absorption peaks in the

blue and the red region of the spectrum.

The beam attenuation coefficient (c) for all samples declined monotonically from

the blue to the red wavelengths and, like the scattering coefficient, did not exhibit a

strong relationship to pigment concentration. Similar to the scattering coefficient, the

beam attenuation coefficient for the 10.6 mg m^{-3} water sample was about twice as high as

for the other samples (Fig. 4C). The scattering coefficient dominated the beam attenuation coefficient ($a + b = c$) at wavelengths above 500 nm. With the exception of the IOPs for the 10.6 mg m^{-3} water sample, the scattering coefficient was not very sensitive to pigment concentration implying a large contribution to the water column IOPs from suspended particles other than phytoplankton, typical of Case 2 waters.

Modeled remote sensing reflectance - Modeled remote sensing reflectance spectra of optically deep water showed an increase in the wavelength of peak emission of the remote sensing reflectance as pigment concentration of the water column increased (Fig. 5). As the pigment concentration of the water column increased from 1.0 to 6.0 mg m^{-3}, the peak wavelengths of the modeled remote sensing reflectance spectra were red-shifted 30 nm. However, the magnitude of this shift decreased with increasing pigment concentration and the wavelength of peak emission shifted only 5 nm as pigment concentration increased from 6.0 to 10.6 mg m^{-3}.

The modeled remote sensing reflectance spectra of optically shallow water revealed the influence of bottom reflectance, in both brightness and spectral shape, as a function of water column IOPs and water depth. In all cases, optically shallow water was brighter than optically deep water. As water column pigment concentration and depth increased, the spectral amplitude and shape of optically shallow waters approached that of optically deep water (Fig. 6).

The predicted remote sensing reflectance of vegetated bottoms at 2 m depth maintained the characteristic shapes of the bottom reflectance spectra at wavelengths below 600 nm in water columns with up to 6 mg m^{-3} total pigment (Figs. 6A-6D).

Remote sensing reflectance in the blue wavelengths was low, compared to bottom

reflectance, due to high absorbance in these wavelengths by CDOM and suspended

particles in the water column. In the water column with 10.6 mg m^{-3} total pigment, the

spectra approached the shape and amplitude of optically deep water (Fig. 6E). The sharp

increase in the absorption coefficient of water from 570 to 600 nm (Morel and Prieur

1977) resulted in a sharp decline at these wavelengths in the remote sensing reflectance

spectra of all bottom types except for that of the brighter coralline algae, which

maintained its shape at wavelengths above 600 nm. The decrease in remote sensing

reflectance from 570 to 600 nm, due to absorption by the water column, served to

truncate the bottom reflectance spectra and created characteristic peaks in the remote

sensing reflectance of the vegetated bottoms (Table 3).

The remote sensing reflectance of the sand bottom was the brightest, with a peak

amplitude that was 1.5 to 2 times brighter than the vegetated bottoms and rose

monotonically until the sharp decline above 570 nm due to water absorption (Fig. 6A).

The spectral peak of sand mirrored that of optically deep water, except for the two

clearest water columns where the sand peak was at a longer wavelength than that of

optically deep water (Figs. 6A-6E). The remote sensing reflectance spectra of the

seagrass bottom maintained their broad peaks with the maximum wavelength fluctuating

from 540 to 565 nm. The remote sensing reflectance spectra of the seagrass and the

coralline red algal bottom, which peaked at 590 nm, were the brightest among the

vegetated bottoms. The remote sensing reflectance spectra of the brown algal bottom,

which peaked at 570 nm, and fleshy red algal bottom were considerably darker than those

of the seagrass and the coralline red algal bottoms. The spectra of the fleshy red algal bottom contained a broad plateau from 540 to 585 nm with a peak that varied within this range and was influenced by the reflectance of optically deep water. This plateau is actually an area of low absorbance in the bottom reflectance spectrum of the fleshy red algae (cf. Fig. 2), but due to low overall reflectance of the fleshy red algae and high absorbance of the red wavelengths by the water column, the interrupted rise from this plateau becomes the spectral peak in the remote sensing reflectance of fleshy red algae.

The water column IOPs had a greater influence on the spectral shapes of the modeled remote sensing reflectance for bottoms of 4 m than those of 2 m (Fig 6F-J). All of the amplitudes were depressed relative to the spectra at 2 m depth, in some cases as much as 50%. The remote sensing reflectance spectra of the different bottom classes were distinguishable at pigment concentrations of 1.0 and 2.4 mg m^{-3}, but the characteristic spectral peaks were depressed (Figs. 6F-6G). The spectra approached the shape and amplitude of the optically deep water spectrum as the pigment concentration of the water column increased to 4.9 and 6.0 mg m^{-3}, except for the sand spectrum, which remained distinct from the optically deep water spectrum (Figs. 6H-6I). The remote sensing reflectance spectra of the vegetated and sand bottoms were essentially identical to that of optically deep water at a pigment concentration of 10.6 mg m^{-3} (Fig. 6J).

Field measurements of remote sensing reflectance - Remote sensing reflectance spectra measured by the HTSRB supported the spectral peak predictions made using radiative transfer calculations (Fig. 7, cf. Fig. 6). Field spectra over seagrass showed a broad plateau from 540 to 565 nm, while those over brown, fleshy red, and coralline red

18

algal bottoms had peaks at 570, 580, and 585 nm respectively. These peaks were similar to modeled predictions and the spectra agreed in shape as well as in general amplitude. The field data shown in Fig. 7 were not all collected under the same environmental conditions and thus show the effect of the water column and depth on spectral amplitude.

The remote sensing reflectance spectra measured with the HTSRB were very similar to model predictions calculated using the same environmental parameters (Fig. 8). Although modeled predictions consistently underestimated the remote sensing reflectance, their amplitude was usually within 50% of the HTSRB measurements. Inconsistencies were most evident in the blue region of the spectrum and probably resulted from errors in the water column IOPs, particularly overestimates of a, supplied to the model.

Analysis of environmental variability and determination of practical detection limits - The error inherent in the amplitude of the field spectra must be accounted for when determining if the amplitudes of two measured spectra, or modeled spectra in this case, are different. Environmental noise resulted in an error of about 1.5 % in the blue and green regions of the spectrum, increasing to 2.5 % in the far red portion of the spectrum (Fig. 9). The error at 550 nm was 2%, so doubling the error produced the minimum detectable difference of 4% between spectra at 550 nm. It is important to note that this detection limit was based entirely on the capacity to distinguish between the amplitude of two spectra at a single wavelength and not on spectral shape.

Using 4% as the minimum difference required to distinguish among the various bottom types, the remote sensing reflectance spectra of vegetated or sand bottoms were

19

distinguishable from those of optically deep water to about 2.1 to 2.7 optical depths, or about 7 to 8 m in water with a pigment concentration of 1.0 mg m^{-3} (Fig. 10A). The geometric depth is the optical depth divided by the downwelling diffuse attenuation coefficient, with K_d supplied by Hydrolight in this study. As the pigment concentration in the water column increased, the detection limit of sand actually increased to 2.7 optical depths, although the corresponding geometric depth decreased from about 8 m to 3.4 m (Fig. 10B). The detection limit between brown or red algal bottoms and optically deep water decreased to 1.5 optical depths in turbid water, or about 2 m. The detection limit of coralline red algal and seagrass from optically deep water was about 2.5 optical depths and was not affected greatly by turbidity, although the geometric depth for coralline red algal bottoms decreased from 7.3 m in the clearest water to 2.7 m in the most turbid water and for green bottoms from 7.5 m to 3.1 m.

The detection limit for distinguishing between the modeled remote sensing reflectance spectra of two vegetation classes, or a vegetative class and sand, ranged from about 2 to 2.5 optical depths, or 14 to 8 % of surface irradiance respectively, for all but the most turbid water (Fig. 10C). The average corresponding geometric depths for all comparisons ranged from 7.3 m in the clearest water to 2.6 m in the most turbid water in this study. The brown and fleshy red algal bottoms could not be distinguished from each other at any depth using the remote sensing reflectance at 550 nm due to the similarity in their bottom reflectances at this wavelength. However, by using the remote sensing reflectance at 570 nm, the fleshy red and brown algal bottoms could be distinguished to

1.3 optical depths, or 4.3 m, in clearer water and to 0.7 optical depths, or less than one meter, in more turbid water (Fig. 10D).

It is the contrast between the reflectance of two different bottom types (A_1-A_2) that drives the limits of distinguishing between the bottoms using remote sensing reflectance. ANCOVA showed that the relationship between bottom contrast and detection depth was significantly different among all pigment concentrations (Fig. 11, Table 4). An LSD post hoc test showed no difference among pigment concentrations of 1.0 mg m^{-3} to 6.0 mg m^{-3} (Table 4). However, the relationship was slightly, though significantly, different in water with a pigment concentration of 10.6 mg m^{-3} than it was for all other pigment concentrations, with the exception of the 2.4 mg m^{-3} water sample. This slight difference is only evident when two bottoms have a relatively low contrast of about 35%.

Benthic identification – The characteristic peak wavelengths of remote sensing reflectance determined in this study (Table 3) were applied to remote sensing reflectance spectra measured by the HTSRB to identify the bottom composition along a transect (Figs. 12A and 12B). The transect progressed from shallow to deep water and the bottom depth beneath the HTSRB ranged from 1.5 to 6.4 m (Fig 12C). Characteristic spectral peaks were easily identified at depths of less than four meters and attributed to underlying benthic vegetation. In some cases, peak wavelengths were intermediate to the characteristic peaks and were assumed to result from mixed pixels, a pixel containing two or more optical classes. However, the issue of mixed pixels was not addressed in this study and this assumption could not be confirmed. The area covered by each spectral

measurement was a function of water depth and boat speed. For example, at three meters depth, an area of less than one square meter was detected by the upwelling radiance detector of the HTSRB.

The amplitudes of the remote sensing spectra were highly variable (Fig. 12D). Higher than normal amplitudes (>0.01) may be attributed to two conditions. Giant kelp suspended between the bottom and the HTSRB upwelling radiance sensor may result in bright brown pixels due to reduced pathlength through the water column. Secondly, sand bottoms may have reflectance spectra with peaks similar to green bottoms and thus be mistaken as a vegetated bottoms. Recall that the peak of the remote sensing reflectance spectrum of a sand bottom can echo that of the water column thus appearing green. However, the brightness of a sand bottom relative to a seagrass bottom should allow proper identification of the two classes. For example, at a depth of four meters, the characteristic spectral peaks became consistent with those of the green optical class, but due to the high amplitude of the reflectance spectra, were more likely due to a sand bottom (Figs. 12B and 12D). The resulting transect of bottom composition was overlaid on a map of the area using GPS coordinates (Fig. 12E).

DISCUSSION

Maritorena et al. (1994) concluded that spectral resolution is the key for proper interpretation of the bottom signature and the results of this study support their conclusion. Hyperspectral sensors, with narrow width bands across the spectrum, are vital for distinguishing between optical classes with small spectral differences that would

22

be averaged together by broad band sensors. A spectral resolution of at least 10 nanometers, and more desirably 5 nanometers, is necessary to identify the classes of submerged benthic vegetation defined here. Identification of lower divisions within these optical classes, especially at the species level, will be difficult, if not impossible, to achieve, due to similarities in spectral shape and amplitude. The results of my study indicate that hyperspectral sensors do provide the detail needed to separate optical classes of macroalgae and seagrass but, due to absorption by the water column, only to depths of about 4 meters in clearer water (with total pigment concentrations of less than 3 mg m^{-3}) and to 2 meters in more turbid water. Using data from an airborne hyperspectral sensor with a 5.5 nm bandwidth, Hochberg and Atkinson (2000) had success separating coral, macroalgae, and sand in a patch reef with a mean water depth of 1.5 meters, but did not attempt to distinguish different optical classes of algae. Even with the advent of hyperspectral data sets, depth remains a limiting factor in discrimination among optical classes of subtidal vegetation and between sand and vegetated bottoms.

Hyperspectral data sets, with their continuous coverage across the spectrum, allow the use of derivative analysis; however, hyperspectral data must be smoothed before derivative analysis is applied to avoid noise in the resulting signal. When data with a resolution of one nanometer or less are smoothed, identifying spectral peaks are retained (Richardson et al. 1994; Hochberg and Atkinson 2000). When the HTSRB data, with a nominal bandwidth of 2.5 nm and binned to 5 nm in this study, were smoothed, the resolution of the spectral peaks needed for identification of the benthic components was lost. Thus, although derivative analysis provides a valuable tool, it did not prove useful

at 5 nm resolution. An additional benefit of the continuous spectral coverage offered by hyperspectral data sets is the availability of alternate wavelengths that can be utilized to separate optical classes when standard wavelengths available on multispectral sensors do not prove useful. For example, in this study, fleshy red and brown algae could not be distinguished using remote sensing reflectance values at 550 nm, which is included in the 545-565 nm band of the SeaWIFS and MODIS sensors, but could be distinguished using values at 570 nm which are not provided by these instruments.

Enhanced spectral resolution enables the detection of the characteristic reflectance peaks of bottom vegetation from its remote sensing reflectance, but its usefulness is limited by the brightness of the bottom, the IOPs of the water column, and the water depth. Low reflectivity of the benthic layer in temperate waters contributes to the difficulty of bottom detection in these environments by decreasing the amount of L_w available for remote sensing detection. Many subtidal macrophytes in Monterey and Carmel Bays live in a low light environment due to the canopy cover of the giant kelp, persistent summer fog, and high levels of phytoplankton in the water column. Lowered light levels can cause the algae to develop an increased concentration of pigment relative to their counterparts in higher light environments (Ramus et al. 1976), which results in darker coloration, increased absorbance, and a consequent decrease in reflectance. Eelgrass in Monterey Bay contains greater concentrations of pigment than turtlegrass (*Thalassia testudinum*) growing in the high light environment of the Bahamas (Cummings and Zimmerman in review) and, as a result, has lower reflectance, at least between 525 and 600 nm (Zimmerman in review). The bottom reflectances of tropical

algae measured by Maritorena et al. (1994) were two to four times brighter than the bottom reflectances measured for corresponding optical classes in this study. Thus, a larger portion of the incident irradiance reaching the benthic layer will be absorbed in these relatively dark environments, subsequently reducing the water leaving radiance available for remote identification of subtidal benthic vegetation.

Water column IOPs define the spectral characteristics of light incident upon the benthic boundary as well as how the light reflected from the bottom is attenuated by the water column as it travels back towards the surface. At wavelengths below 600 nm, the absorption coefficient is determined primarily by the water column constituents and not by the absorbance of water itself. Many remote sensing studies have focused on the ability to detect benthic vegetation or coral reefs in clear, tropical waters where wavelengths shorter than 600 nm are not strongly absorbed due to much lower concentrations of chlorophyll, detritus, and CDOM than in temperate waters. The absorption coefficients of CDOM measured in this study were an order of magnitude larger than those recorded by Boss and Zaneveld (in press) in the oligotrophic Bahamian water. Diminished CDOM concentration leads to lowered absorption of the blue wavelengths by the water column resulting in a peak in the remote sensing reflectance of optically deep water in the blue portion of the spectrum (Dierssen and Smith 2000). In oligotrophic waters where there is little absorption due to chlorophyll, detritus, and CDOM, the remote sensing reflectance spectra of a carbonate sand bottom contains a blue peak at 495 nm (Dierssen et al. in press; Louchard et al. in press), similar to that of optically deep water, which contrasts strongly with the peaks between 530 and 600 nm in

the remote sensing reflectance of vegetated bottoms. In clear Bahamian water, Dierssen et al. (in press) were clearly able to distinguish the remote sensing reflectance spectra of sand and seagrass with peaks at 495 and 540 nm respectively. This contrast is the basis for ocean color remote sensing in optically deep water, where the ratio of the water leaving radiance of blue and green wavelengths is used to determine the pigment concentration of the water (Gordon et al. 1983).

In more turbid waters, absorption by chlorophyll, detritus, and CDOM increase the total absorption coefficient at wavelengths below 550 nm shifting the peak in the remote sensing reflectance of optically deep water to the green and yellow wavelengths and making it more difficult to distinguish the characteristic peaks of macroalgae and seagrass from optically deep water. From Equation 1 it is apparent that the contrast between bottom reflectance and the reflectance of optically deep water drives the contribution of the bottom reflectance in the remote sensing reflectance signal. Thus, key wavelengths of the remote sensing reflectance spectrum of vegetated bottoms will be more difficult to distinguish from those of optically deep water when high concentrations of suspended and dissolved matter in the water column shift the spectral peaks to longer wavelengths characteristic of benthic vegetation (Figs. 4 and 7). The peak wavelength of the remote sensing reflectance of sand will also be shifted to longer wavelengths (Fig. 6, Table 3) making it more difficult to determine sand bottoms from vegetated bottoms. However, the large amplitude of its reflectance should allow sand to be distinguished from optically deep water as well as vegetated bottoms.

The strong absorption by water at wavelengths beyond 600 nm is independent of the water column constituents. In more turbid water, the absorption coefficient at these wavelengths is increased further by contributions from chlorophyll. Although these wavelengths have proved useful for the development of algorithms to identify the benthic layer with data collected in situ (Holden and LeDrew 1999), in the intertidal (Bajjouk et al. 1996), or in very shallow water (Alberotanza et al. 1999), they lose their usefulness in remotely sensed data at 4 to 5 m depth in clear oceanic waters, and at 1 to 2 m depth in turbid coastal water (Kutser et al. 2000). My study showed that identifiable features beyond 600 nm disappeared quickly at depths beyond 2 m. Despite their limited use for identification of subtidal vegetation, wavelengths beyond 600 nm may provide valuable for applications such as bathymetry retrieval (Dierssen et al. in press).

In temperate environments, characterized by highly variable water column turbidity, remote sensing collections should be planned for periods when water clarity is at its highest. In Monterey Bay, seasonal upwelling in spring and summer provide high nutrients that stimulate phytoplankton growth. Upwelling generally begins in March or April and continues through August or September, although the northwest winds responsible for upwelling can maintain high surface chlorophyll levels through November (Pennington and Chavez 2000). Hauschildt (1985) noted that after the onset of the non-upwelling season in September 1982, there was reappearance of upwelling in October probably due to increases in wind stress. My data show high pigment levels through October 1999 when northwest winds were evident (http://www.mbari.org/bog/nopp/coamps/subregion/default.htm). Thus, remote sensing

data collections would best be planned for the winter months in Monterey Bay when the chlorophyll concentrations are generally the lowest.

Modeled data, confirmed by field measurements, were used to reach the conclusions of this study. In comparisons between theoretical and field data, the radiative transfer model often underestimated the remote sensing reflectance, which may be due to inaccuracies in the measurement of water column IOPs, a parameter of vital importance to the model. It is possible that the CDOM absorption coefficients were too high for some samples because of particle contamination of the CDOM filtrate. This contamination may have occurred from chlorophyll and detritus passing through the filter pad as the CDOM filtrate was collected. CDOM absorption influences the blue wavelengths of the spectrum, the region where the largest discrepancies between modeled and field spectra occurred. Use of an instrument such as WET Labs ac-9 (WET Labs, Inc.), which measures a and c at nine wavelengths, may prevent such error, but does not allow for measurements with small spectral resolution (1-nm in this study), the determination of the separate absorption components (a_p and a_y), or for the analysis of pigment concentration.

Another factor contributing to incorrect predictions may have been the morphology and canopy architecture of the in situ benthic vegetation. Hydrolight assumes that the bottom is a Lambertian reflector and, in this study, the bottom reflectance used for the model came from an average measure of seaweed thalli or seagrass leaves oriented normally to the measuring beam of a spectrophotometer. In nature algal and seagrass canopies are not Lambertian reflectors, and plant morphology

creates vertical structure within the canopy that significantly affects the canopy leaving radiance (Zimmerman in review). Mobley et al. (in press) determined that for most remote sensing reflectance purposes, the assumption of a Lambertian bottom for horizontal surfaces results in less than a ten percent error in the model predictions. However, the solar zenith angle at the time the remote sensing measurement is made may affect the accuracy of this assumption (Voss et al. in press). Thus, further work on the architecture of submerged plant canopies is needed to analyze the discrepancy between model predictions and field observations.

My results indicate that identification of benthic optical classes in temperate environments may be made to a depth of two to four meters, depending on water clarity. The use of remote sensing for the mapping of submerged aquatic vegetation thus has good potential in the shallow subtidal. Ackleson and Klemas (1987) suggest that masking known optically deep water may help eliminate confusion between the remote sensing reflectance of dense submerged aquatic vegetation and optically deep water. This method may prove useful when the peak wavelength of the remote sensing reflectance of optically deep water is similar to that of benthic vegetation. Although not apparent in the modeled data, the field measurements of optically deep water in this study always displayed a rise towards 400 nm in the remote sensing reflectance spectra which might also be used to distinguish optically deep water from vegetated bottoms (Figs. 8C and 8D).

Despite the depth limitations, there are several potential applications of hyperspectral remote sensing in the shallow subtidal environment. If possible, remote

sensing overflights should be planned during seasons of optimal water clarity, such as the winter months in Monterey Bay, to increase the geometric depth of optically shallow water. Remote sensing can be a useful tool for mapping seagrass, which only grows to about a depth of ten percent surface irradiance or 2.3 optical depths (Duarte 1991), within the detection limits found in this study to distinguish seagrass and sand. Additionally, vegetation in the shallow subtidal may be more susceptible to natural and anthropogenic disturbance than deeper vegetation and remote sensing may be useful to monitor such changes. Finally, remote sensing can be used to map the large areas of macroalgae in the rocky intertidal and shallow subtidal in areas such as the central coast of California, that are inaccessible and difficult to survey using traditional methods. Continued research could establish hyperspectral remote sensing as an important tool for ecological assessment and management of the shallow subtidal environment.

LITERATURE CITED

Abbott, I. A., and G. J. Hollenberg. 1976. Marine algae of California. Stanford University Press.

Ackleson, S. G., and V. Klemas. 1987. Remote sensing of submerged aquatic vegetation in Lower Chesapeake Bay: A comparison of Landsat MSS to TM Imagery. Remote Sensing of Environment, **22:** 235-248.

Alberotanza, L., V. E. Brando, G. Ravagnan, and A. Zandonella. 1999. Hyperspectral aerial images. A valuable tool for submerged vegetation recognition in the Orbetello Lagoons, Italy. Int. J. Remote Sensing, **20:** 523-533.

Armstrong, R. A. 1993. Remote sensing of submerged vegetation canopies for biomass estimation. Int. J. Remote Sensing, **14:** 621-627.

Bajjouk, T., B. Guillaumont, and J. Populus. 1996. Application of airborne imaging spectrometry system data to intertidal seaweed classification and mapping. Hydrobiol., **326/327:** 463-471.

Bochkov, B. F., O. V. Kopelevich, and B. A. Kriman. 1980. A spectrophotometer for investigating the light extinction by sea water in the visible and ultraviolet regions of the spectrum. Oceanology, **20:** 101-104.

Boss, E., and J. R. V. Zaneveld. In press. The effect of bottom substrate on inherent optical properties: Evidence of biogeochemical processes. Limnol. Oceanogr.

Cleveland, J. S., and A. D. Weidemann. 1993. Quantifying absorption by aquatic

  particles: A multiple correction for glass-fiber filters. Limnol. Oceanogr.,

  38: 1321-1327.

Cummings, M. E., and R. C. Zimmerman. In review. Submarine irradiance, light

  harvesting and the package effect in seagrasses: Optical constraints on

  photoacclimation. Aquat. Bot.

Demetriades-Shah T. H., M. D. Steven, and J. A. Clark. 1990. High resolution

  derivative spectra in remote sensing. Remote Sens. Environ., **33:** 55-64.

Deysher, L. E. 1993. Evaluation of remote sensing techniques for monitoring

  giant kelp populations. Hydrobiol., **260/261:** 307-312.

Dierssen, H. M., and R. C. Smith. 2000. Bio-optical properties and remote sensing

  ocean color algorithms for Antarctic Peninsula waters. J. Geophys. Res.,

  105: 26,301-26,312.

Dierssen, H. M., R. C. Zimmerman, R. A. Leathers, T. V. Downes, and C. O.

  Davis. In press. Remote sensing of seagrass and bathymetry in the

  Bahamas Banks using high resolution airborne imagery. Limnol.

  Oceanogr.

Duarte, C. M. 1991. Seagrass depth limits. Aquat. Bot., **40:** 363-377.

Foster, M. S., and D. R. Schiel. 1985. The ecology of giant kelp forests in

  California: a community profile. U.S. Fish Wildl. Serv. Biol. Rep. 85(7.2).

Gordon, H. R., D. K. Clark, J. W. Brown, O. B. Brown, R. H. Evans, and W. W.
Broenkow. 1983. Phytoplankton pigment concentrations in the Middle
Atlantic Bight: comparison of ship determinations and CZCS estimates.
Appl. Opt., **22:** 20-36.

Govindjee, and B. Z. Braun, 1974.   Light absorption, emission and
photosynthesis. In: W. D. P. Stewart [ed.], Algal physiology and
biochemistry, University of California Press, 346-390.

Hauschildt, K. S. 1985 . Remotely sensed surface chlorophyll and temperature
distributions off central California and their potential relations to
commercial fish catches. M. S. Thesis, San Francisco State University.

Hemminga, M. A., and C. M. Duarte. 2000. Seagrass Ecology. Cambridge
University Press.

Hernández-Carmona, G., Y. E. Rodríguez-Montesinos, J. R. Torres Villegas, I.
Sánchez Rodríguez, and M. A. Vilchis. 1989. Evaluation of *Macrocystis*
pyrifera (Phaeophyta, Laminariales) kelp beds in Baja California, Mexico.
I. Winter 1985-1986. Ciencias Mar., **15:** 1-27.

Hochberg, E. J., and M. J. Atkinson. 2000. Spectral discrimination of coral reef
benthic communities. Coral Reefs, **19:** 164-171.

Holden, H., and E. LeDrew. 1999. Hyperspectral identification of coral reef
features. Int. J. Remote Sensing, **20:** 2545-2563.

Hughes, T. 1994. Catastrophes, phase shifts, and large-scale degradation of a
Caribbean coral reef. Science, **265:** 1547-1551.

Jensen, J. R., J. E. Estes, and L. Tinney. 1980. Remote sensing techniques for kelp surveys. Photogram. Eng. Remote Sens., **46**: 743-755.

Jousson, O., J. Pawlowski, L. Zaninetti, F. W. Zechman, F. Dini, G. Di Guiseppe, R. Woodfield, A. Millar, and A. Meinesz. 2000. Invasive alga reaches California. Nature, **408**: 157-158.

Jupp, D. L. B., K. K. Mayo, D. A. Kuchler, D. V. R. Classen, R. A. Kenchington, and P. R. Guerin. 1985. Remote sensing for planning and managing the Great Barrier Reef of Australia. Photogram., **40**: 21-42.

Kaiser, J. 2000. California algae may be feared European species. Science, **289**: 222-223.

Kirk, J. T. O. 1994. Light and photosynthesis in aquatic ecosystems. Cambridge University Press.

Knight, D., E. LeDrew, and H. Holden. 1997. Mapping submerged corals in Fiji from remote sensing and in situ measurements: applications for integrated coastal management. Ocean Coast. Mgmt., **34**: 153-170.

Kutser, T., J. Parslow, L. Clementson, W. Skirving, T. Done, M. Wakeford, and I. Miller. 2000. Hyperspectral detection of coral reef bottom types. Ocean Optics XV, edited by S. Ackleson and J. Marra. Office of Naval Research.

Louchard, E. M., R. P. Reid, C. F. Stephens, C. O. Davis, R. A. Leathers, and T. V. Downes. In press. Optical remote sensing of benthic habitats and bathymetry in coastal environments at Lee Stocking Island, Bahamas: A comparative spectral classification approach. Limnol. Oceanogr.

Malthus, T. J., and D. G. George. 1997. Airborne remote sensing of macrophytes in Cefni Reservoir, Anglesey, UK. Aquat. Bot., **58:** 317-332.

Maritorena, S., A. Morel, and B. Gentili. 1994. Diffuse reflectance of oceanic shallow waters: influence of water depth and bottom albedo. Limnology and Oceanography, **39:** 1689-1703.

Meinesz, A., J. de Vaugelas, B. Hesse, and X. Mari. 1993. Spread of the introduced tropical green alga *Caulerpa taxifolia* in northern Mediterranean waters. J. Appl. Phycol., **5:** 141-147.

Mobley, C. D. 1989. A numerical model for the computation of radiance distribution in natural waters with wind-roughened surfaces. Limnol. Oceanogr., **34:** 1473-1483.

Mobley, C. D., and L. K. Sundman. In press. Effects of optically shallow bottoms on upwelling radiances: Inhomogeneous and sloping bottoms. Limnol. Oceanogr.

Morel, A., and L. Prieur. 1977. Analysis of variations in ocean colour. Limnol. Oceanogr., **22:** 709-722.

Mumby, P. J., E. P. Green, A. J. Edwards, and C. D. Clark. 1997. Coral reef habitat-mapping: how much detail can remote sensing provide? Mar. Biol., **130:** 193-202.

Pennington, J. T., and F. P. Chavez. 2000. Seasonal fluctuations of temperature, salinity, nitrate, chlorophyll and primary production at station H3/M1 over 1989-1996 in Monterey Bay, California. Deep-Sea Res. II, **47:** 947-973.

Peñuelas, J., J. A. Gamon, K. L. Griffin, and C. B. Field. 1993. Assessing

community type, plant biomass, pigment composition, and photosynthetic

efficiency of aquatic vegetation from the spectral reflectance. Remote

Sens. Environ., **46**: 110-118.

Price, J. C. 1994. How unique are spectral signatures? Remote Sens. Environ., **49**:

181-186.

Ramus, J., I. Beale, D. Mauzerall, and K. L. Howard. 1976. Changes in

photosynthetic pigment concentration in seaweeds as a function of water

depth. Mar. Biol., **37**: 223-229.

Richardson, L. L., D. Buisson, C. Liu, and V. Ambrosia. 1994. The detection of

algal photosynthetic accessory pigments using airborne visible-infrared

imaging spectrometer (AVIRIS) spectral data. Mar. Tech. Soc. J., **28**: 10-

21.

Strickland, J. D. H., and T. R. Parsons. 1972. A Practical Handbook for Seawater

Analysis. Fish. Res. Bd. Can.. Bull. 167.

Voss, K. J., C. D. Mobley, L. K. Sundman, J. Ivey, and C. Mazell. In press. The

spectral upwelling radiance distribution in optically shallow waters.

Limnol. Oceanogr.

Willard, H. H., L. L. Merritt, Jr., and J. A. Dean. 1974. Instrumental Methods of

Analysis. D. Van Nostrand Company.

Zimmerman, R. C. In review. Radiative transfer and photosynthesis in seagrass

canopies. Limnol. Oceanogr.

Table 1. Definitions and units of variables.

Variable	Units	Definition
A	dimensionless	Albedo or bottom reflectance
a_t	m^{-1}	Total absorption coefficient: $a_p + a_w + a_y$
a_p	m^{-1}	Particle absorption coefficient
a_w	m^{-1}	Pure water absorption coefficient
a_y	m^{-1}	CDOM absorption coefficient
b	m^{-1}	Scattering coefficient
c_t	m^{-1}	Total beam attenuation coefficient: $a + b$
c_w	m^{-1}	Pure water beam attenuation coefficient
E_d	$W\ m^{-2}\ nm^{-1}$	Downwelling irradiance
E_u	$W\ m^{-2}\ nm^{-1}$	Upwelling irradiance
H	m	bottom depth
K	m^{-1}	Diffuse attenuation coefficient
K_d	m^{-1}	Downwelling diffuse attenuation coefficient
L_u	$W\ m^{-2}\ nm^{-1}$	Upwelling radiance
L_w	$W\ m^{-2}\ nm^{-1}$	Water leaving radiance
R	dimensionless	Reflectance
R_b	dimensionless	Bottom reflectance
R_{rs}	sr^{-1}	Remote sensing reflectance
R_∞	dimensionless	Reflectance of optically deep water
z	m	Bottom depth
λ	nm	Wavelength

Table 2. Species list of macroalgae and seagrass used to compute the average spectral reflectance of each optical class.

FLESHY RED ALGAE	CORALLINE RED ALGAE	BROWN ALGAE	SEAGRASS
Callophyllis violacea	*Bossiella sp.*	*Cystoseira osmundacea*	*Zostera marina*
Chondracanthus corymbiferus	*Calliarthron tuberculosum*	*Desmarestia ligulata*	
Chondracanthus harveyanus	*Mesophyllum conchatum*	*Dictyoneuropsis reticulata*	
Cryptopleura lobulifera		*Dictyoneurum californicum*	
Cryptopleura ruprechtiana		*Laminaria farlowii*	
Mazzaella lilacina		*Laminaria setchelli*	
Prionitis sp.		*Macrocystis pyrifera*	
Rhodymenia californica		*Pterygophora californica*	

Table 3. The wavelength of peak emission of modeled remote sensing reflectance spectra for each optical class. A) 2 m depth. B) 4 m depth

A.

Optical class	Pigment concentration of the water column (mg m^{-3})				
	1.0	2.4	4.9	6.0	10.6
Brown algae	570	570	565	570	575
Red algae	540	560	560	585	575
Coralline algae	590	590	590	590	585
Seagrass	540	555	555	565	570
Sand	570	565	560	570	575
Optically deep water	540	560	560	570	575

B.

Optical class	Pigment concentration of the water column (mg m^{-3})				
	1.0	2.4	4.9	6.0	10.6
Brown algae	565	570	560	570	575
Red algae	540	560	560	570	575
Coralline algae	540	560	560	580	575
Seagrass	540	560	560	570	575
Sand	565	565	560	570	575
Optically deep water	540	560	560	570	575

Table 4. Upper table shows ANCOVA results testing effect of pigment concentration on logarithmic relationship between bottom contrast and optical depth of detection limit. Lower table displays results of a LSD Post Hoc Test for differences among pigment concentrations.

* indicates a significant difference at $p = 0.05$.

ANCOVA

df Effect	MS Effect	df Error	MS Error	F	p-level
4	0.088	29	0.025	3.57	0.017*

POST HOC TEST p values

	2.4 mg m-3	4.9 mg m-3	6.0 mg m-3	10.6 mg m-3
1.0 mg m-3	0.285	0.684	0.695	0.005*
2.4 mg m-3		0.503	0.148	0.066
4.9 mg m-3			0.426	0.015*
6.0 mg m-3				0.002*
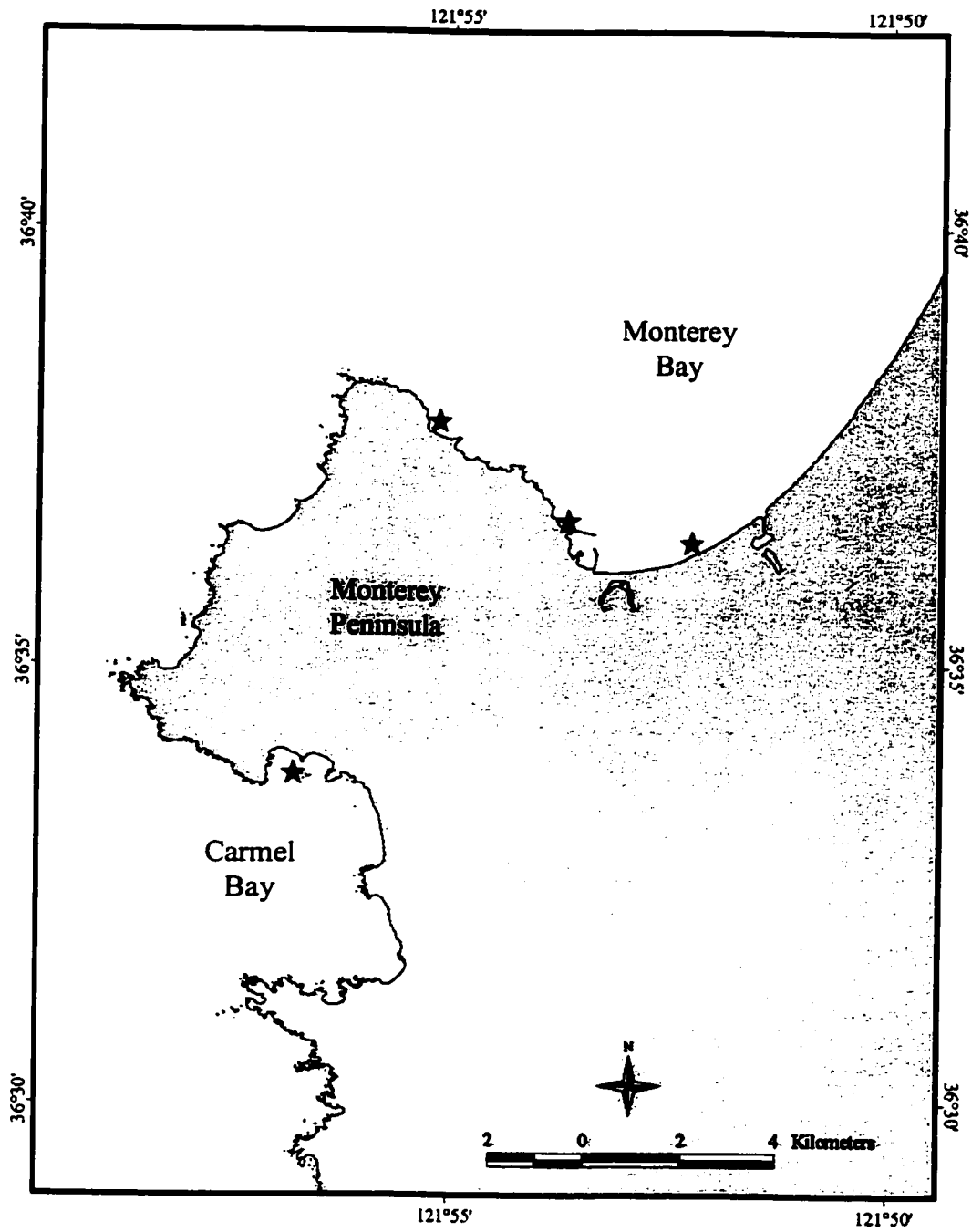
Figure 1. Site map of the study area with primary sites marked with stars.
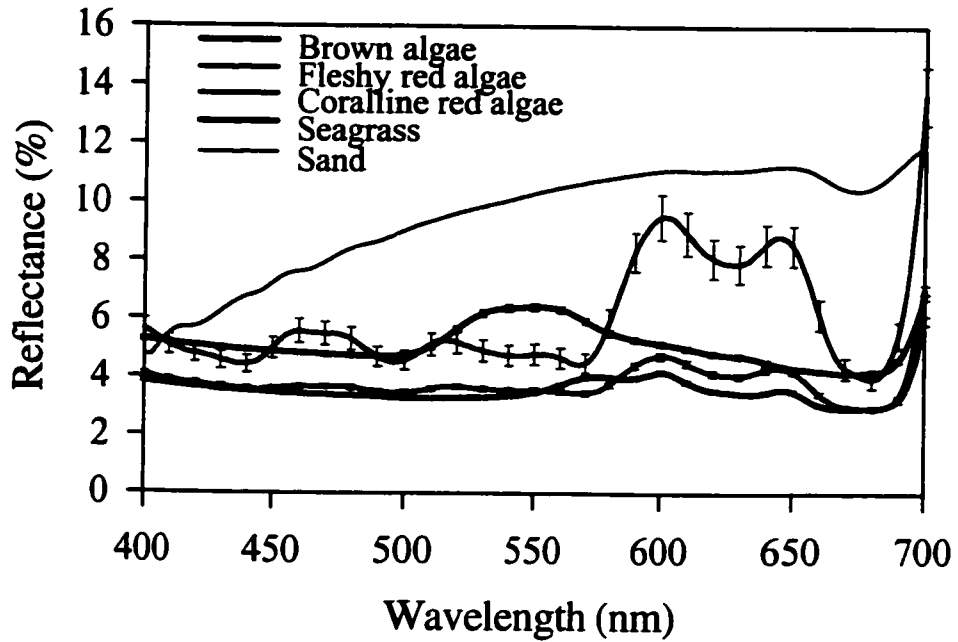
Figure 2. Average spectral reflectance of brown, fleshy red and coralline red macroalgae, the seagrass *Zostera marina*, and a sand sample from Stillwater Cove. Error bars are standard error. Although error was calculated for each nanometer, it is only shown at ten nanometer intervals.
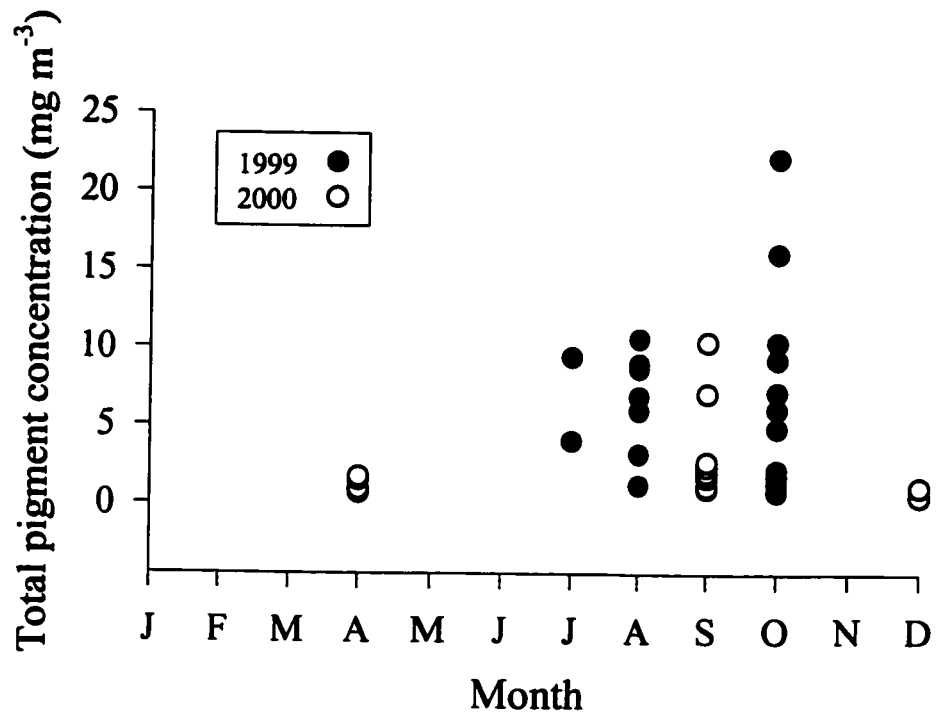
Figure 3. Total pigment concentration (the combined concentrations of chlorophyll a and phaeopigment) for water samples collected from July 1999 to December 2000.
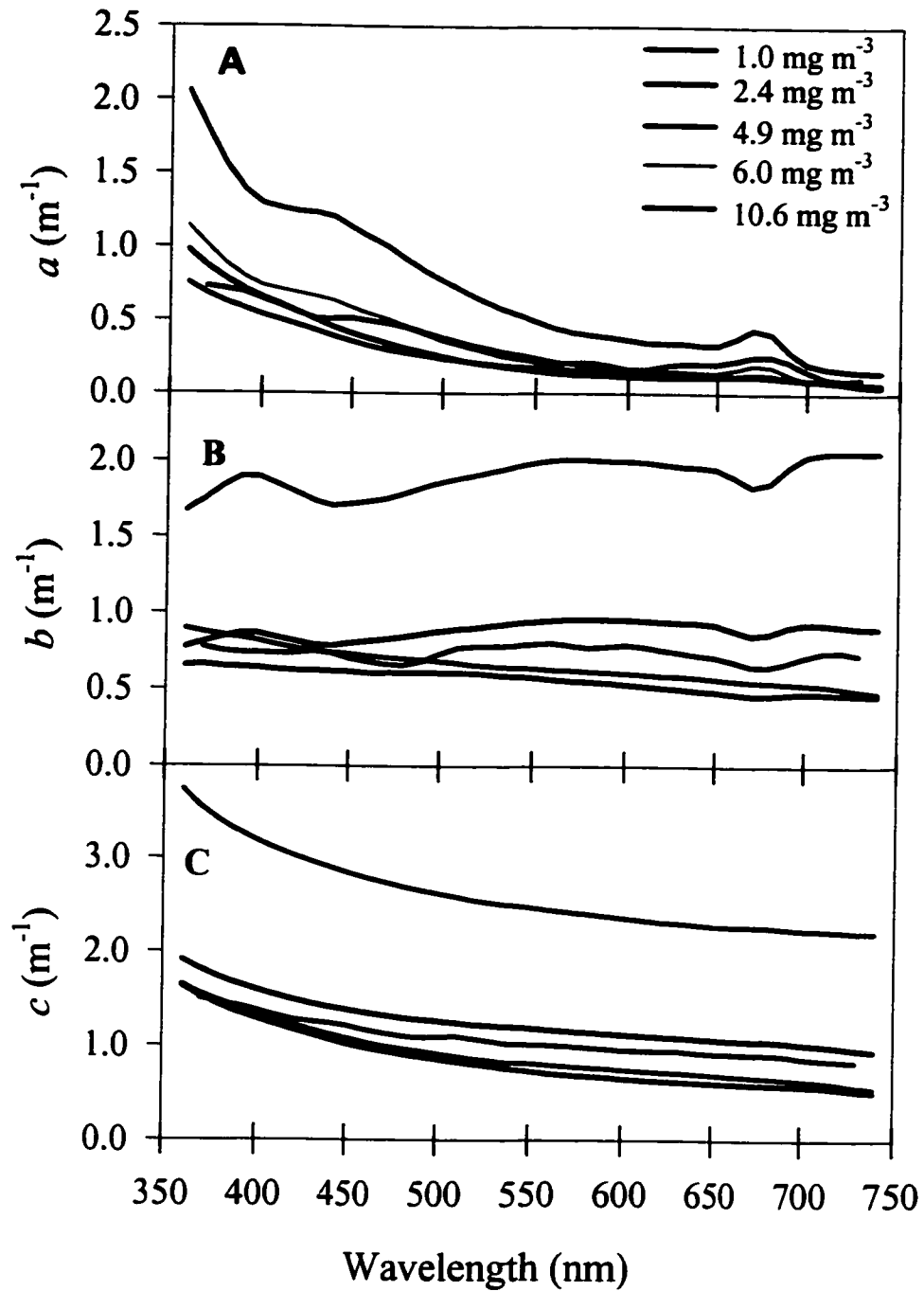
Figure 4. A) Absorption coefficients without water. B) Scattering coefficients without water. C) Beam attenuation coefficients without water.

44
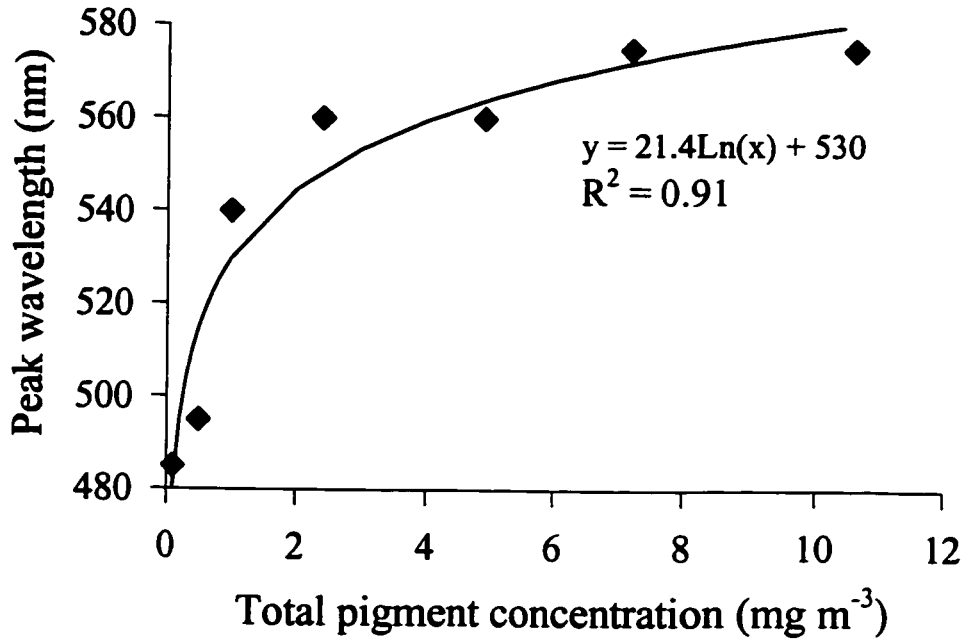
Figure 5. The relationship between the wavelength of peak emission of modeled remote sensing reflectance (R_{rs}) spectra of optically deep water and the total pigment concentration of the water column.

The plotted regression is given by:

$$y = 21.4\text{Ln}(x) + 530$$
$$R^2 = 0.91$$
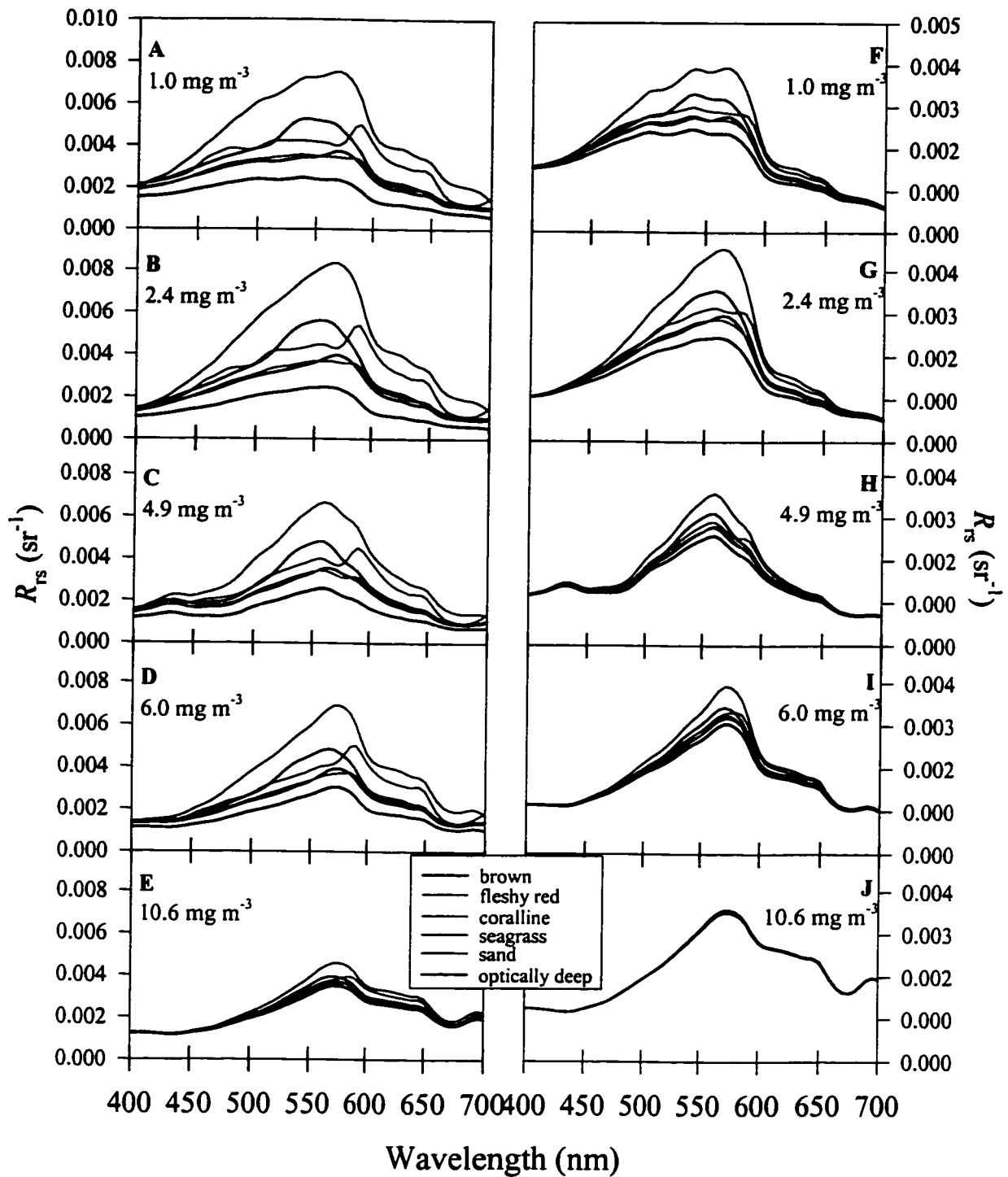
Figure 6. Remote sensing reflectance (R_{rs}) spectra predicted by the radiative transfer model Hydrolight for six bottom reflectances in water columns with a total pigment concentration ranging from 1.0 mg m^{-3} to 10.6 mg m^{-3} noted on each graph. Bottom depth was 2 meters for graphs A - E and 4 meters for graphs F - J. Note different scales on y-axis between the graphs of each depth.
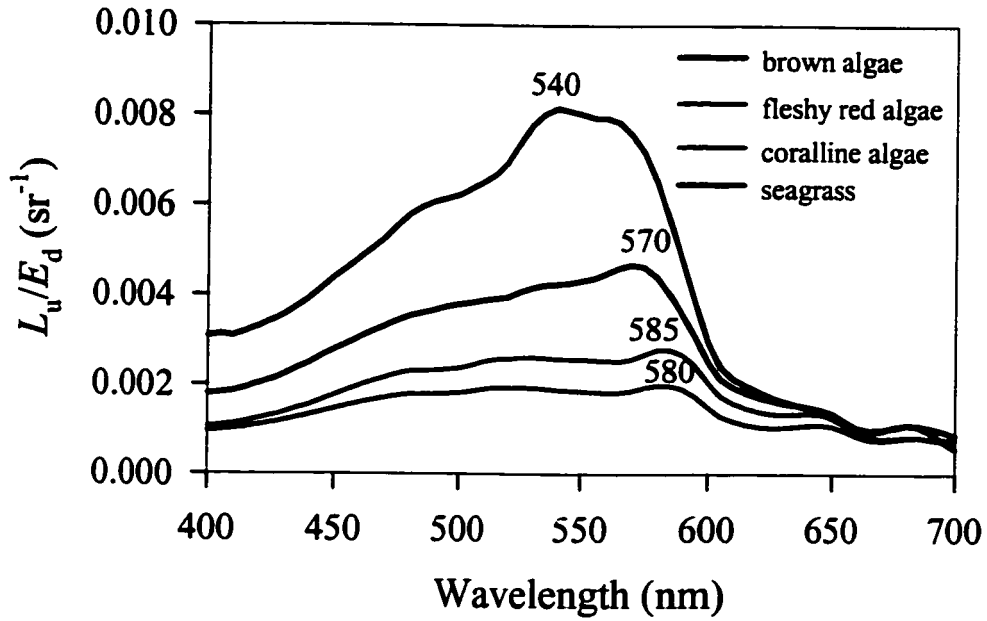
Figure 7. Field measurements of remote sensing reflectance (L_u/E_d) measured by the HTSRB over different vegetated bottoms indicated in the legend. Water column IOPs and depth were not consistent for these measurements. The number over each spectrum indicates the wavelength of peak reflectance
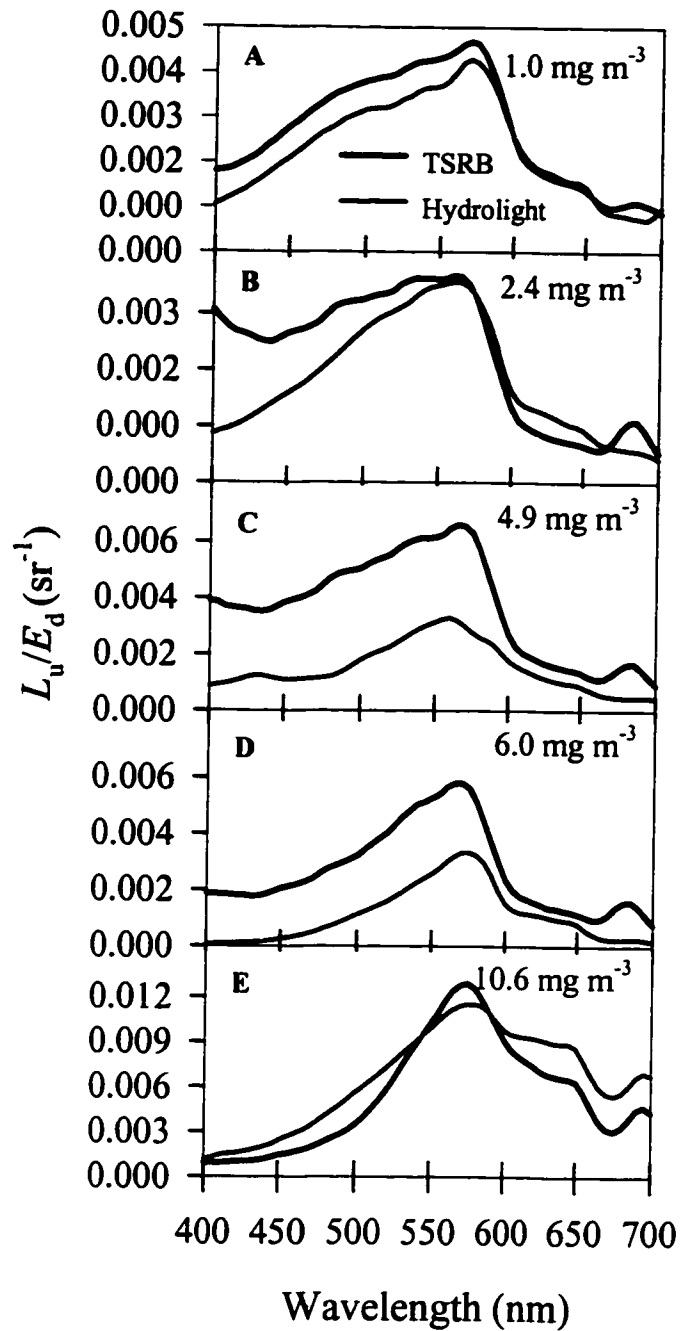
Figure 8. Comparisons of modeled and measured remote sensing reflectance (L_u/E_d) in water columns with total pigment concentrations noted on each graph.
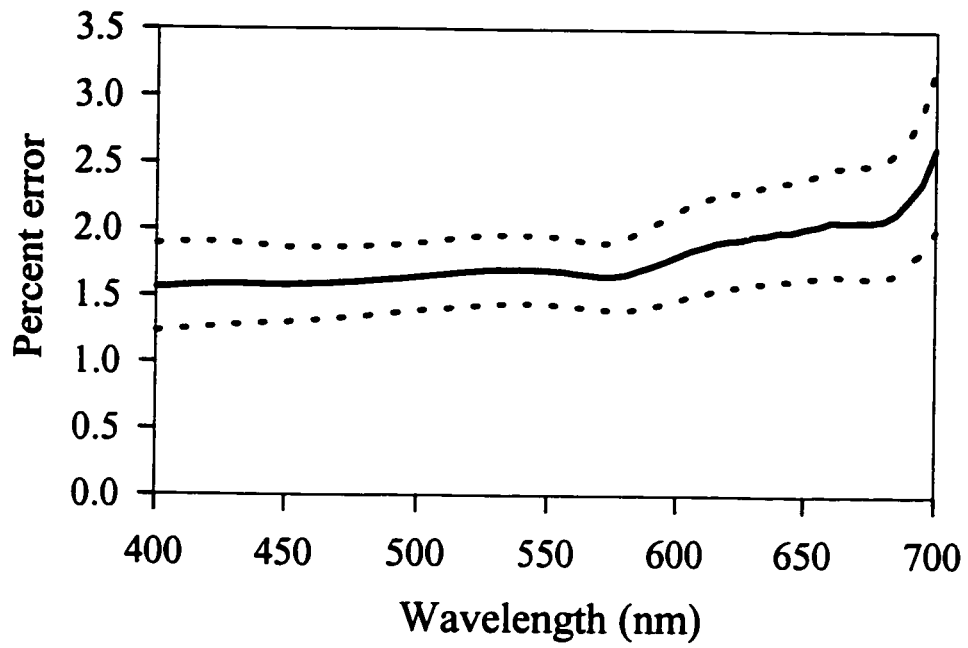
Figure 9. Mean percent error of twenty-one HTSRB data files resulting from environmental noise. Dashed lines represent the 95% confidence interval.
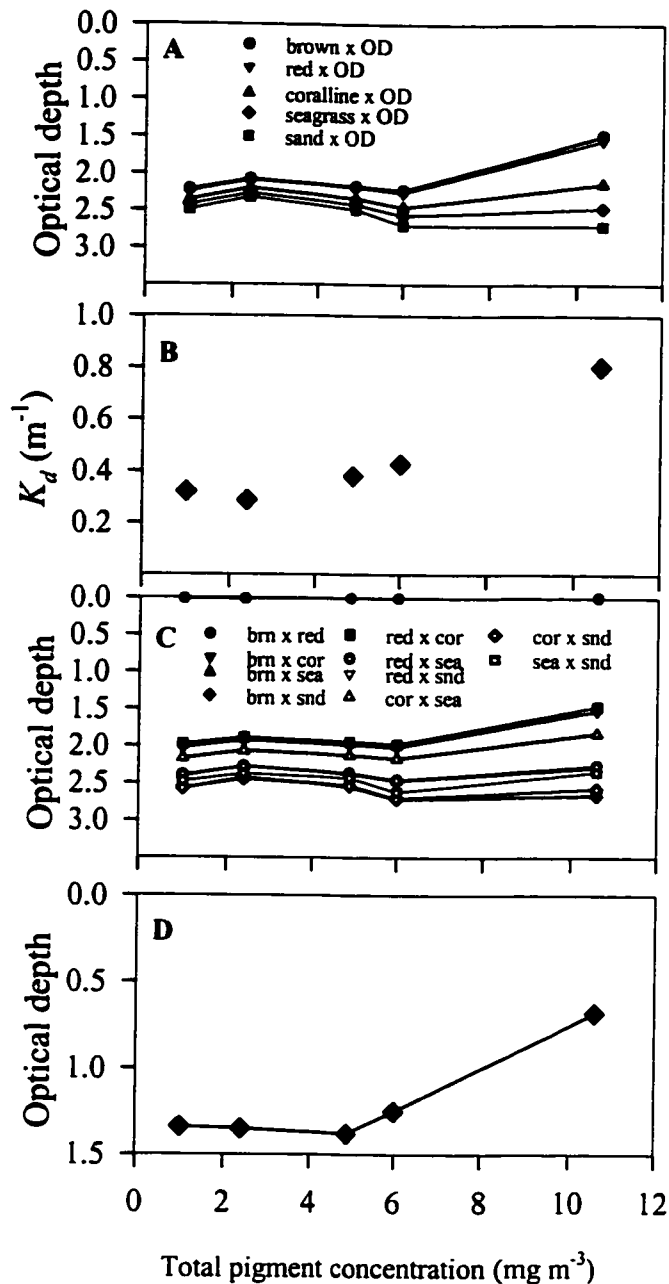
Figure 10. A) Optical depth of the detection limit between modeled remote sensing reflectance (R_{rs}) spectra (based on a 4% difference at 550 nm) as a function of total pigment concentration of the water column for vegetated and sand bottoms vs. optically deep water. B) The relationship between the total pigment concentration of the water and the downward diffuse attenuation coefficient (K_d). C) Optical depth of the detection limit between modeled remote sensing reflectance (R_{rs}) spectra (based on a 4% difference at 550 nm) as a function of total pigment concentration of the water column for vegetated and sand bottoms vs. one another. D) Optical depth of detection limit between modeled remote sensing reflectance (R_{rs}) spectra (based on a 4% difference at 570 nm) of brown and fleshy red algal bottoms
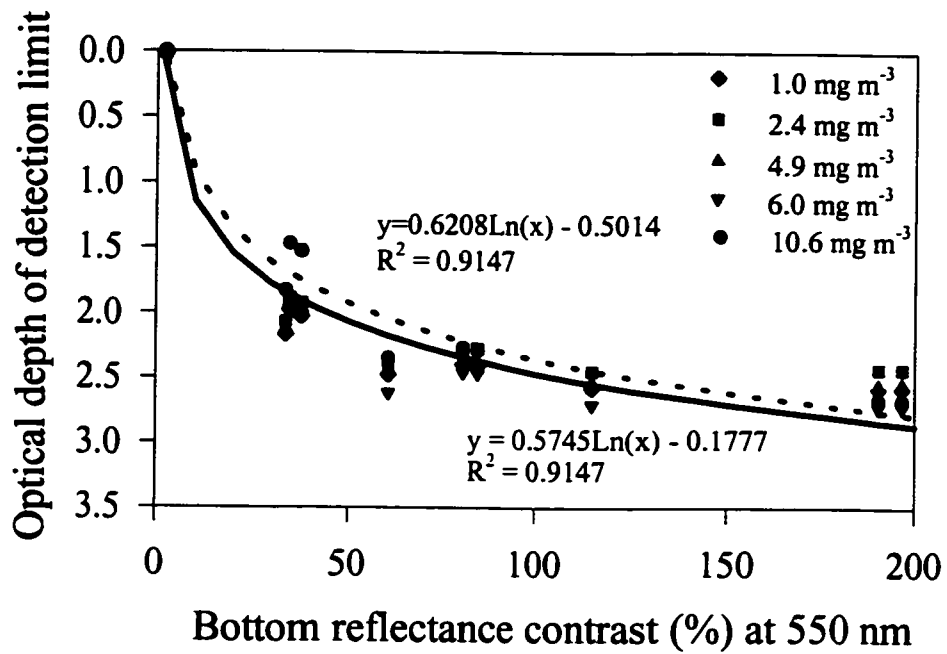
Figure 11. The relationship of percent contrast between two bottom reflectances at 550 nm and the optical depth of detection limit between modeled remote sensing reflectance (R_{rs}) spectra. Detection limit based on a 4% difference in R_{rs} at 550 nm.
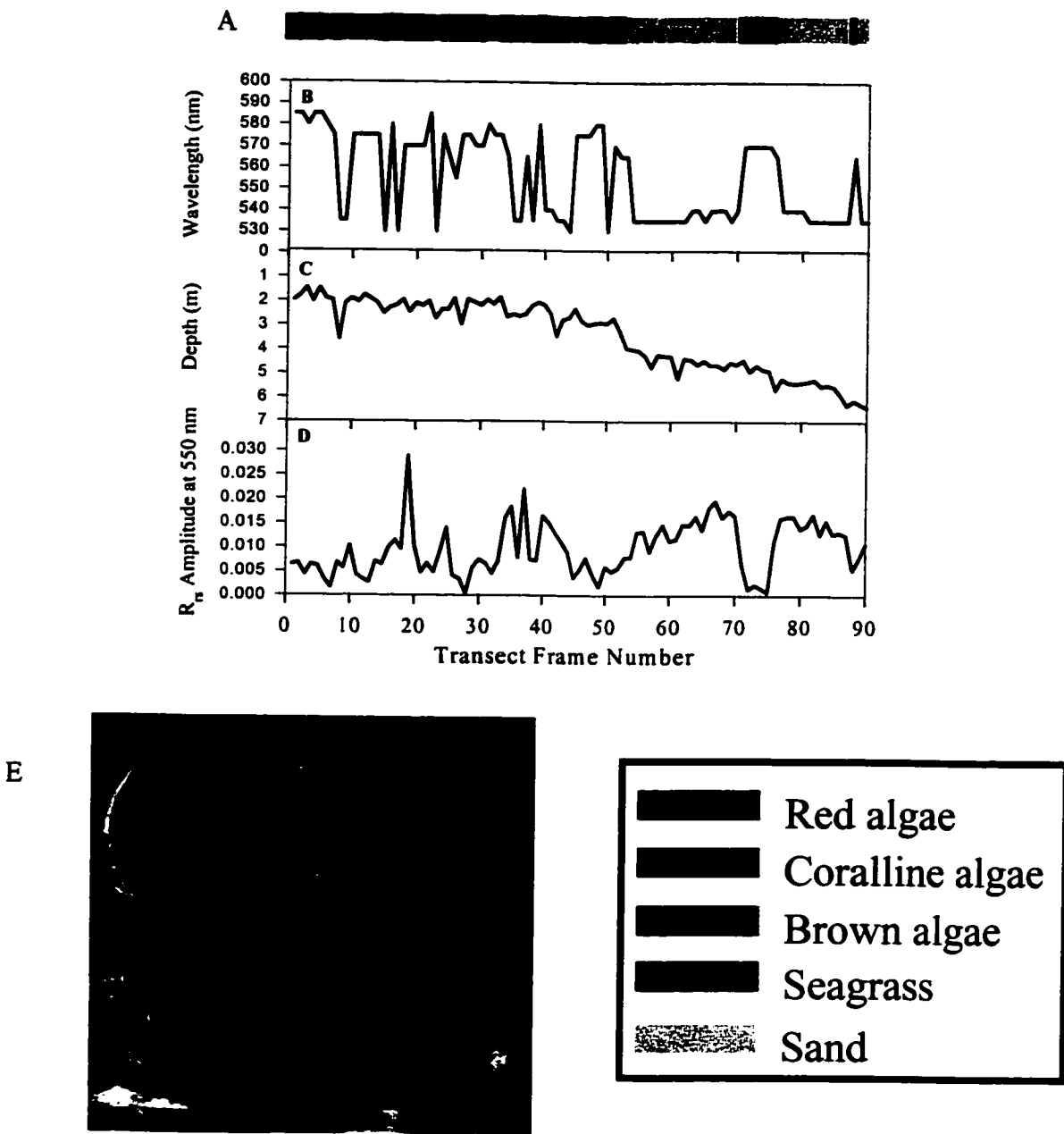
Figure 12. A) Bottom composition along a 90 m transect in Stillwater Cove. Each frame represents about a length of 1 m and a width of 0.6 m, with the width enlarged relative to length for ease of viewing. The legend at the bottom of the page indicates bottom vegetation with intermediate colors assumed to be mixed pixels. B) The peak wavelength between 530 and 600 nm of HTSRB measured remote sensing reflectance from which bottom composition was determined. C) The depth measured from the HTSRB sensor to the bottom. D) The amplitude of the remote sensing reflectance signal at 550 nm. E) The transect of benthic vegetation overlaid on a false color image of remotely sensed data from a remote sensing aircraft overflight to show position within Stillwater Cove.

52
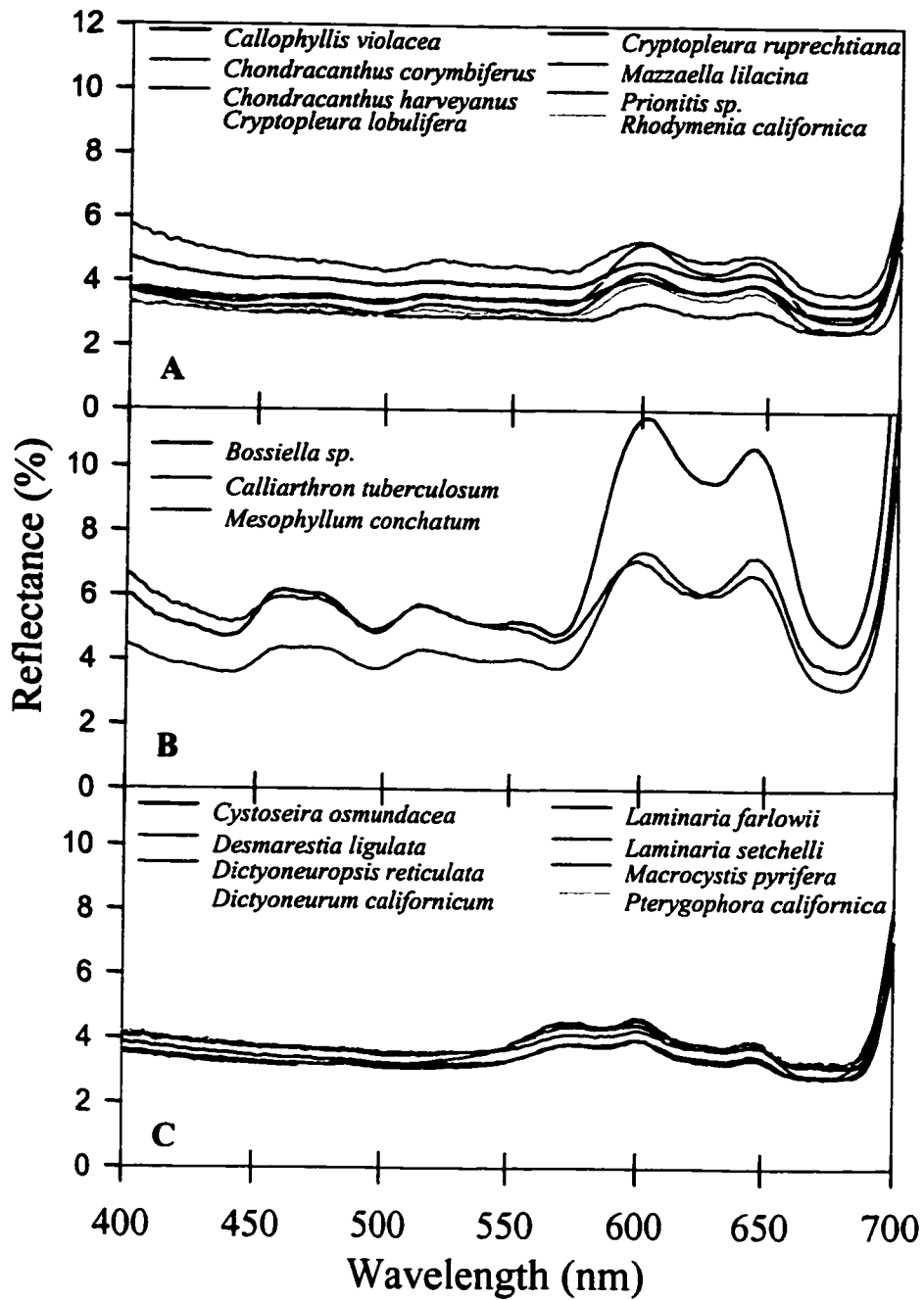
Appendix 1. Complete spectral library of A) fleshy red algae, B) coralline red algae, and C) brown algae.